DOI: 10.1002/ejic.201001072

[FeFe]-Hydrogenase Models: Unexpected Variation in Protonation Rate between Dithiolate Bridge Analogues

Aušra Jablonskytė,[a] Joseph A. Wright,[a] and Christopher J. Pickett*[a]

Keywords: [FeFe]-Hydrogenase / Metalloenzymes / Protonation / Kinetics / Reaction mechanisms

The model [FeFe]-hydrogenase subsite $Fe_2(\mu\text{-odt})(CO)_4(PMe_3)_2$ (odt = 2-oxapropane-1,3-dithiolate) has been crystallized for the first time, revealing an apical–basal arrangement of the two phosphane groups. Protonation of this species has been studied by a combination of stopped-flow ultraviolet and infrared techniques along with time-resolved NMR spectroscopy. The kinetics of the protonation are similar to those for $Fe_2(\mu\text{-edt})(CO)_4(PMe_3)_2$ (edt = ethane-1,2-dithiolate) and are much slower than those for the protonation of $Fe_2(\mu\text{-pdt})(CO)_4(PMe_3)_2$ (pdt = propane-1,3-dithiolate). The dithiolate bridge length is therefore not the key determinant of reactivity in these simple model systems.

Introduction

The [FeFe]-hydrogenase has attracted a great deal of interest from the bio- and synthetic inorganic communities over the recent years.[1] The native enzyme catalyzes the formation of dihydrogen gas from protons and electrons with very high efficiency, comparable to that of platinum-based fuel cells.[2] Reproducing this activity in synthetic models is a significant challenge, and a number of research groups are currently pursuing competent models.[1,3]

The active site of the enzyme features a {2Fe2S} sub-site bound to a {4Fe4S} electron-transfer unit (Figure 1). This presents two key questions: the initial site of protonation (terminal vs. bridging hydride) and the nature of the central atom in the dithiolate ligand. Using ^1H NMR spectroscopy at low temperature, Rauchfuss and co-workers have observed terminal hydrides as intermediates in the protonation of model complexes bearing the dppv [1,2-bis(diphenylphosphanyl)ethylene] ligand,[4] and have suggested that this points to terminal intermediates in almost all cases.[5] However, the generality of a terminally bound intermediate is yet to be conclusively determined. On the identity of X, Lubitz and co-workers have presented HYSCORE evidence in favour of NH,[6,7] whereas Szilagyi has argued for a central oxygen atom.[8] Further understanding of this intriguing question is vital for a complete picture of the reaction mechanism of the [FeFe]-hydrogenase.

We have recently reported stopped-flow kinetic studies on models for the [FeFe]-hydrogenase bearing either all-carbon dithiolate bridges (**1** and **2**, Figure 2)[9,10] or containing a central nitrogen atom (**3**, Figure 2).[11] Kinetics derived from time-resolved infrared and ultraviolet studies show that protonation of **1** and **2** follows the same general mechanism. The first observed product is a bridging hydride in which at least one phosphane is in the apical position; a slow isomerisation then takes place to give the thermodynamically favored bridging hydride in which the phosphanes are *transoid*-dibasal. Notably, both steps of the reaction were an order of magnitude *slower* for **2** than for **1**. Reaction of **3** with protons occurs first at the nitrogen atom, followed by a slow conversion to the same bridging hydride isomer as is seen for the all-carbon analogues.

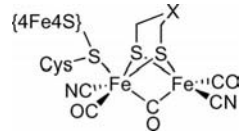

Figure 1. Active sub-site in the native enzyme (X = CH_2, NH or O).

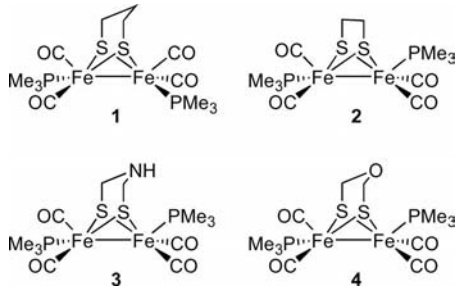

Figure 2. Model for the [FeFe]-hydrogenase sub-site.

[a] Energy Materials Laboratory, School of Chemistry, University of East Anglia,
Norwich NR4 7TJ, United Kingdom
Fax: +44-1603-592-003
E-mail: c.pickett@uea.ac.uk

Here, we report the synthesis and protonation kinetics of the oxygen-containing dithiolate-bridged system **4**, completing the series of related X-atom variants to be investigated by stopped-flow methods. The kinetic data show that even the apparently subtle difference between CH_2 and O has major mechanistic implications.

Results and Discussion

The oxygen-bearing dithiolate-bridged model **4** has not previously been reported, although the precursor $Fe_2[\mu\text{-}(SCH_2)_2O](CO)_6$ has been described.[12] Reaction to form **4** from this precursor is analogous to the formation of **1** and **2**,[13,14] and proceeds smoothly. The crude material was crystallized from hexanes to give **4** as a red powder in moderate yield (30%). Cooling of a concentrated hexane solution of this purified material gave a crystalline solid, which was examined by X-ray diffraction (Figure 3). This revealed that in the solid state one of the PMe_3 groups in **4** is in the basal position, whereas the second is apical. The crystal structure of **1** shows that it features two basal phosphanes,[15] whereas **2**, which bears a less bulky dithiolate ligand, exhibits the same apical–basal arrangement as seen in **4**.[14] The solid-state structure of **3** has not been reported to date, but a number of *N*-alkylated analogues, in which one phosphane is apical, have been crystallized.[16–19] The metal–metal bond length in **4** [2.5235(5) Å] is similar to that in **2** [2.5159(6) Å], and both are significantly shorter than the distance in **1** [2.555(2) Å]. In the same way, the average Fe–S–Fe angle in **1** [69.12(11)°] is larger than in **2** [67.91(3)°] or **4** [67.81(3)°]. Interestingly, these metrics parallel rates of both protonation and isomerization (vide infra). As a comparison, in the enzymatic system the Fe–Fe bond length is 2.6 Å and the Fe–S–Fe angle is 68°.[20,21] Complex **1** with the longer metal–metal bond and wider Fe–S–Fe average angle is the fastest-reacting system.

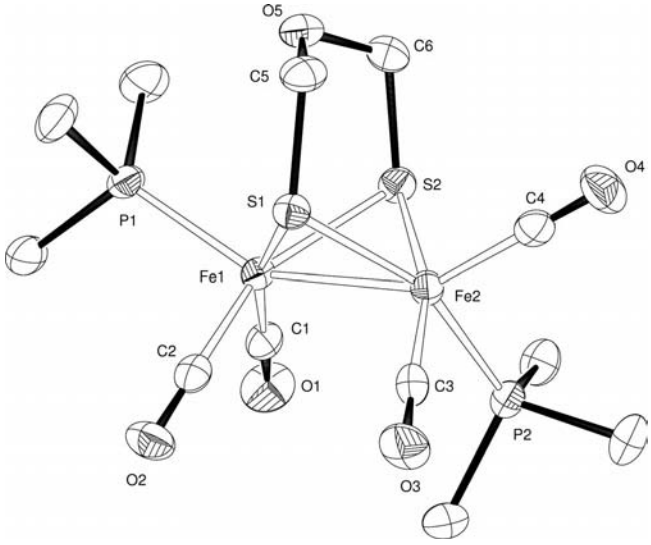

Figure 3. ORTEP representation of the structure of **4** showing 50% probability ellipsoids; hydrogen atoms have been omitted for clarity.

Compound **4** exhibits strong absorption in the UV region at 372 nm, which is lost on protonation. The rate of the reaction of **4** with $HBF_4{\cdot}Et_2O$ in MeCN can therefore be conveniently monitored by using stopped-flow UV spectroscopy. In a range of acid concentrations between 50 and 500 mM the loss of the signal of the starting material follows pseudo-first-order kinetics, which can be fitted by a single exponential decay (Figure 4).

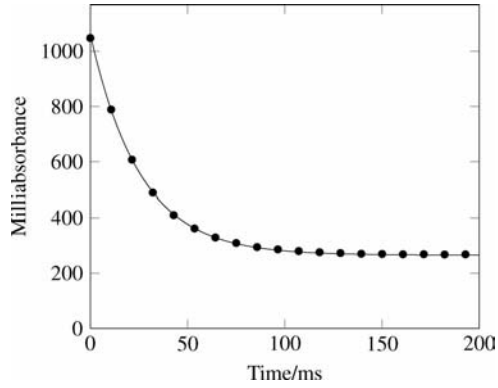

Figure 4. Decay of the UV signal at 372 nm on protonation of **4** (circles); exponential fit (line). $[\mathbf{4}]_0$ = 0.125 mM, $[HBF_4{\cdot}Et_2O]_0$ = 375 mM.

To verify that this decay was indeed due to the initial protonation step in the reaction, the same process was studied by stopped-flow IR spectroscopy. The starting material shows carbonyl stretches at 1898, 1913, 1947 and 1984 cm^{-1} in MeCN, whereas the final product exhibits stretches at 1997 and 2037 cm^{-1}. These peak positions are very similar to those observed for **1** and its protonation product:[9] the presence of an electron-withdrawing oxygen atom in the dithiolate bridge therefore has a minimal influence on the electron density at the metal atoms. Stopped-flow experiments revealed that, as is the case with **1** and **2**, the reaction can be divided into two phases, an initial protonation with loss of starting material and a slower acid-independent isomerization to the final product (Figure 5).

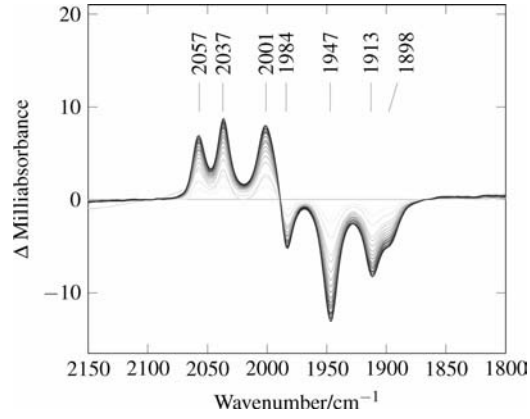

Figure 5. Difference spectrum for the protonation of **4** as observed by stopped-flow IR spectroscopy, in the time range 0.12 s (light grey) to 1.50 s (black) vs. a scan at 40 ms. $[\mathbf{4}]_0$ = 0.50 mM, $[HBF_4{\cdot}Et_2O]$ = 25 mM.

The rate of the first step could be calculated by monitoring the loss of starting material at 1947 cm^{-1}, which again showed pseudo-first-order kinetics.

By combining the UV and IR data, the rate of the initial protonation reaction shows a first-order dependence on the acid concentration over the range studied (Figure 6). The data also confirm that the loss of intensity in the UV spectra is concordant with conversion of the starting material to the protonated product observed in the IR spectra. The rate constant for this process, k_1, is (102 ± 2) $dm^3 mol^{-1} s^{-1}$, similar to that for compound **2**, and around an order of magnitude slower than that observed for compound **1**.[10,22]

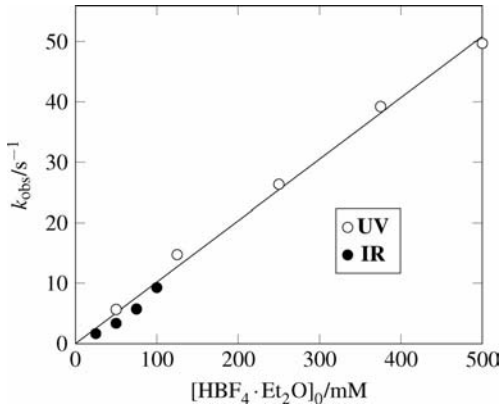

Figure 6. Comparison of rate of reaction of **4** with acid as observed by UV and IR stopped-flow techniques. $[\mathbf{4}]_0$ = 0.125 mM (UV), 0.50 mM (IR).

The second phase of the reaction, isomerization to the final product, was sufficiently slow that it could be monitored by $^{31}P\{^1H\}$ NMR spectroscopy (Figure 7). At short times, four separate signals were visible in the spectrum, which were assigned to three isomeric forms of the protonated product (Figure 8). Two mutually coupled doublets at δ = 24.73 and 28.91 ppm (J = 8.2 Hz) can be assigned as the apical–basal isomer $\mathbf{5}_{ap–ba}$, while two singlets at δ = 24.48 and 25.23 ppm can be assigned as the apical–apical ($\mathbf{5}_{ap–ap}$) and *transoid*-dibasal (*transoid*-$\mathbf{5}_{ba–ba}$) isomers, respectively. This analysis is confirmed by ^1H NMR spectra for the reaction. The first signal observed is a singlet at δ = –14.55 ppm, which can be assigned to $\mathbf{5}_{ap–ap}$. This is converted into a double at δ = –14.70 ppm (J = 23.0 Hz), assignable as $\mathbf{5}_{ap–ba}$, and finally to a triplet at δ = –13.40 ppm (J = 22.0 Hz) due to *transoid*-$\mathbf{5}_{ba–ba}$.[23] The time course in Figure 7 gives a qualitative picture of the evolution of the isomerisation processes. Limitations on sensitivity preclude a detailed analysis. Nevertheless, it is clear that $\mathbf{5}_{ap–ap}$ converts to the *transoid*-$\mathbf{5}_{ba–ba}$ form via $\mathbf{5}_{ap–ba}$. Extrapolation of the experimental values to the time of addition of acid indicates that both $\mathbf{5}_{ap–ap}$ and $\mathbf{5}_{ap–ba}$. are formed directly by the protonation pathway.

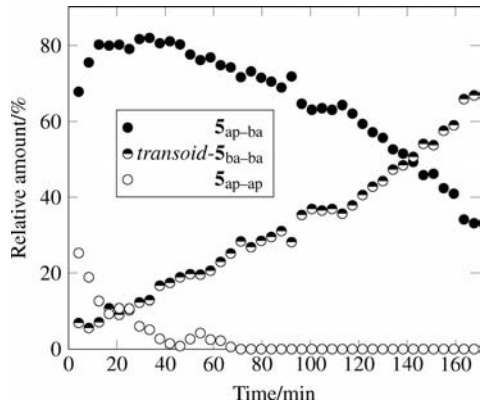

Figure 7. Time course of the reaction of **4** with $HBF_4 \cdot Et_2O$ in $[D_3]$-MeCN; percentages of total integration from $^{31}P\{^1H\}$ NMR spectra; time relative to the first scan (approximately 4 min after addition of the acid). $[\mathbf{4}]_0$ = 10 mM, $[HBF_4 \cdot Et_2O]_0$ = 70 mM.

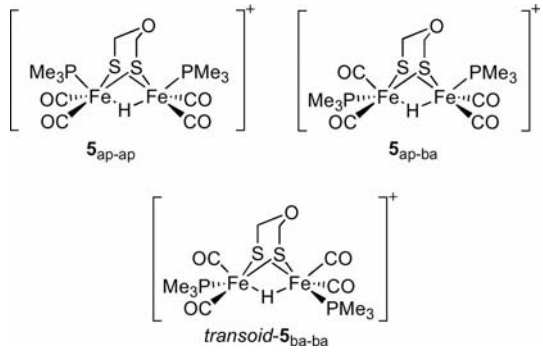

Figure 8. Isomers of **5** observed by $^{31}P\{^1H\}$ NMR spectroscopy.

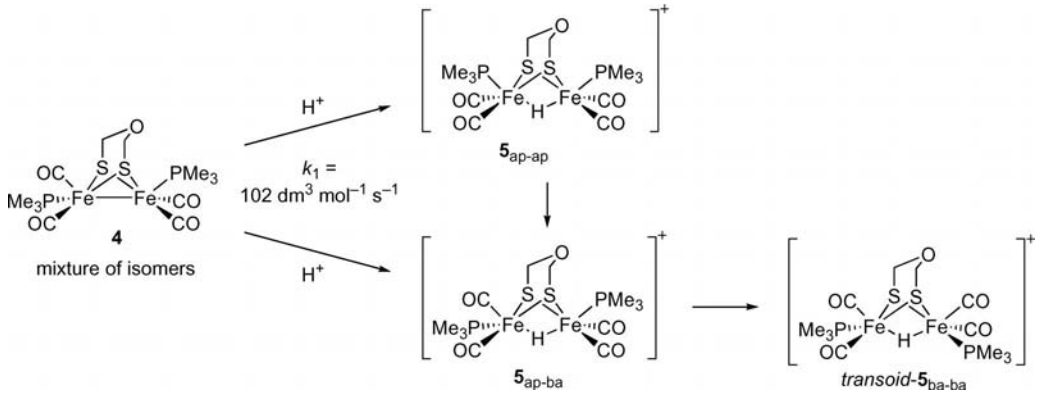

Scheme 1. Proposed reaction mechanism.

It is clear that the dithiolate bridge length alone is not the key determinant of reactivity. Both **1** and **4** feature a three-atom dithiolate bridge, but, while an apical–apical isomer is observed in the protonation of **4**, this is not the case for **1**. In contrast, the initial reaction of **2** with protons does show clear evidence for an apical–apical isomer and occurs at a rate similar to that of **4**. Subsequent isomerisation to the thermodynamic products is fastest for the reaction starting from **1**, around an order of magnitude slower starting from **2** and even more retarded for reaction from **4**.

A mechanism for this process is presented in Scheme 1. The starting material **4** exists in solution as a mixture of isomers,[24] and initial protonation takes place to give either $\mathbf{5}_{ap–ap}$ or $\mathbf{5}_{ap–ba}$ as the first products observed. These protonation routes must have similar rate constants in order to account for the pseudo-first-order kinetics seen experimentally. Rotation then takes place to convert $\mathbf{5}_{ap–ap}$ into $\mathbf{5}_{ap–ba}$ and then into the thermodynamic product *transoid*-$\mathbf{5}_{ba–ba}$. The involvement of a low concentration of *cisoid*-$\mathbf{5}_{ba–ba}$ cannot be ruled out: traces of this isomer are observed in the reaction of both **1** and **2** with protons.

Conclusions

We are left with the open question as to why the protonation rate for **1** is significantly faster than those of **2** or **4**. It is striking that the rates for both initial protonation and subsequent isomerization are both around an order of magnitude slower in **2** and **4** than in **1**. This suggests that there may be a common feature to the two stages of the mechanism, which affects the rate of both processes. The dithiolate bridge length is probably not a key determinant in the reaction mechanism, nor is the electronic influence of CH_2 vs. O, noting the minimal influence of this change on the infrared frequencies of parent and product species. Structurally, it is noteworthy, as mentioned earlier, that **2** and **4** have the shorter metal–metal bonds and the tighter Fe–S–Fe bond angles, both indicative of a stronger Fe–Fe bond. This may play a role in bridging hydride formation and isomerization.

Recently, Hall and co-workers have provided a detailed density functional theory (DFT) examination of the protonation of **1** and have shown a role for basally disposed terminal hydride intermediates,[25] and such studies for **2** and **4** will provide insight into the control that the dithiolate bridge has on protonation and isomerization rates.

Experimental Section

General: Unless otherwise stated, reactions were carried out by using standard techniques for air-sensitive compounds. Solvents were degassed by using a nitrogen purge and dried by using an M. Braun solvent purifier unit before use. Starting materials were purchased from Aldrich or Alfa Aesar and were used without further purification. $Fe_2[\mu\text{-}(SCH_2)_2O](CO)_6$ was prepared according to literature methods.[12] Stopped-flow and time-resolved experiments were carried out as described previously.[10,11]

$Fe_2[\mu\text{-}(SCH_2)_2O](CO)_4(PMe_3)_2$ (4): Trimethylphosphane (0.30 mL, 2.9 mmol) was added to a solution of $Fe_2[\mu\text{-}(SCH_2)_2O](CO)_6$ (205 mg, 0.53 mmol) in hexane (50 mL). The solution was heated to reflux for 1 h, after which time it became dark red. Filtration through Celite followed by removal of the solvent in vacuo afforded the crude product as a red powder. It was purified by cooling the concentrated hexane solution to –30 °C. The resulting red powder (77 mg, 30%) could be recrystallized from hexane to give crystals of **4** suitable for X-ray diffraction. $C_{12}H_{22}Fe_2O_5P_2S_2$ (483.73): calcd. C 29.77, H 4.58; found C 29.80, H 4.48. IR (hexane): $\tilde{\nu}$ = 1992, 1957, 1920 (CO) cm^{-1}. ^1H NMR (300 MHz, CD_2Cl_2, 25 °C): δ = 4.16 (s, 4 H, CH_2), 1.52 (d, $^2J_{P,H}$ = 9.1 Hz, 18 H, CH_3) ppm. $^{31}P\{^1H\}$ NMR (300 MHz, CD_2Cl_2, 25 °C): δ = 21.70 (s, PMe_3) ppm. EI-MS: *m*/*z* = 483.9 [M^+]; calcd. for $C_{12}H_{22}O_5{}^{54}Fe^{56}FeP_2S_2$ 481.9124, found 481.9124.

X-ray Crystallography: From a sample of **4** under oil, a single crystal of ca. 0.53 mm × 0.30 mm × 0.20 mm was mounted on a glass fiber and fixed in the cold nitrogen stream of an Oxford Diffraction Xcalibur-3 CCD diffractometer equipped with Mo-K_α radiation and graphite monochromator. Intensity data were measured by ω-scans. Data were processed by using the CrysAlisPro[26] program. The structure was determined by the direct methods routines in SIR-92[27] and refined by full-matrix least-squares methods on F^2 in SHELXL.[28] Non-hydrogen atoms were refined with anisotropic thermal parameters. Hydrogen atoms were included in idealised positions and set to ride with their U_{iso} values on the parent carbon atoms with their U_{eq} values. CCDC-795961 contains the supplementary crystallographic data for this paper. These data can be obtained free of charge from The Cambridge Crystallographic Data Centre via www.ccdc.cam.ac.uk/data_request/cif.

Acknowledgments

The authors thank the Biotechnology and Biological Sciences Research Council (BBSRC) and the Engineering and Physical Sciences Research Council (EPSRC), the Royal Society and the Wolfson Foundation for funding.

[1] C. Tard, C. J. Pickett, *Chem. Rev.* **2009**, *109*, 2245–2274.
[2] M. W. W. Adams, *Biochim. Biophys. Acta* **1990**, *1020*, 115–145.
[3] F. Gloaguen, T. B. Rauchfuss, *Chem. Soc. Rev.* **2009**, *38*, 100–108.
[4] B. E. Barton, T. B. Rauchfuss, *Inorg. Chem.* **2008**, *47*, 2261–2263.
[5] B. E. Barton, G. Zampella, A. K. Justice, L. De Gioia, T. B. Rauchfuss, S. R. Wilson, *Dalton Trans.* **2010**, *39*, 3011–3019.
[6] S. Foerster, S. M. van Gastel, M. Brecht, W. Lubitz, *J. Biol. Inorg. Chem.* **2005**, *10*, 51–62.
[7] M. Brecht, M. van Gastel, T. Buhrke, B. Friedrich, W. Lubitz, *J. Am. Chem. Soc.* **2003**, *125*, 13075–13083.
[8] A. S. Pandey, T. V. Harris, L. J. Giles, J. W. Peters, R. K. Szilagyi, *J. Am. Chem. Soc.* **2008**, *130*, 4533–4540.
[9] J. A. Wright, C. J. Pickett, *Chem. Commun.* **2009**, *45*, 5719–5721.
[10] A. Jablonskytė, J. A. Wright, C. J. Pickett, *Dalton Trans.* **2010**, *39*, 3026–3034.
[11] J. A. Wright, L. Webster, A. Jablonskytė, P. M. Woi, S. K. Ibrahim, C. J. Pickett, *Faraday Discuss.* **2011**, DOI: 10.1039/c004692b.
[12] L. C. Song, Z. Y. Yang, H. Z. Bian, Y. Liu, H. T. Wang, X. F. Liu, Q. M. Hu, *Organometallics* **2005**, *24*, 6126–6135.
[13] P. Li, M. Wang, C. He, G. Li, X. Liu, C. Chen, B. Åkermark, L. Sun, *Eur. J. Inorg. Chem.* **2005**, 2506–2513.

[14] X. Zhao, I. P. Georgakaki, M. L. Miller, R. Mejia-Rodriguez, C.-Y. Chiang, M. Y. Darensbourg, *Inorg. Chem.* **2002**, *41*, 3917–3928.
[15] X. Zhao, I. P. Georgakaki, M. L. Miller, J. C. Yarbrough, M. Y. Darensbourg, *J. Am. Chem. Soc.* **2001**, *123*, 9710–9711.
[16] L. Schwartz, G. Eilers, L. Eriksson, A. Gogoll, R. Lomoth, S. Ott, *Chem. Commun.* **2006**, 520–522.
[17] W. Dong, M. Wang, X. Liu, K. Jin, G. Li, F. Wang, L. Sun, *Chem. Commun.* **2006**, 305–307.
[18] W. Dong, M. Wang, T. Liu, X. Liu, K. Jin, L. Sun, *J. Inorg. Biochem.* **2007**, *101*, 506–513.
[19] Y. Si, C. Ma, M. Hu, H. Chen, C. Chen, Q. Liu, *New J. Chem.* **2007**, *31*, 1448–1454.
[20] J. W. Peters, W. N. Lanzilotta, B. J. Lemon, L. C. Seefeldt, *Science* **1998**, *282*, 1853–1858.
[21] Y. Nicolet, C. Piras, P. Legrand, C. E. Hatchikian, J. C. Fontecilla-Camps, *Structure* **1999**, *7*, 13–23.
[22] The rate of the initial protonation of **3** is significantly slower than any of the other models, but **3** is very rapidly protonated at the nitrogen atom. This means that the bridge protonation is occurring on an already charged species rather than the neutral compound.
[23] There is little or no coupling between the bridging hydride and the apical phosphane ligands, see for example ref.[9] This means that the position of the phosphane ligands is readily assigned from the multiplicity of the hydride signals in the ^{1}H NMR spectroscopy.
[24] At room temperature, the $^{31}P\{^{1}H\}$ NMR spectrum for **4** shows a single peak at δ = 21.79 ppm. On cooling to –60 °C, this splits into broad signals at δ = 19.90 and 27.12 ppm and a sharp signal at δ = 28.34 ppm, demonstrating that more than one isomer is present in solution.
[25] M. B. Hall, C. Liu, personal communications.
[26] *CrysAlisPro*, Oxford Diffraction Ltd., Abingdon, UK, **2010**.
[27] A. Altomare, G. Cascarano, C. Giacovazzo, A. Guagliardi, *J. Appl. Crystallogr.* **1993**, *26*, 343–350.
[28] G. M. Sheldrick, *Acta Crystallogr., Sect. A: Found. Crystallogr.* **2008**, *64*, 112–122.

Received: October 8, 2010
Published Online: November 15, 2010

